Frequency ratio of Yb and Sr clocks with 5×10⁻¹⁷ uncertainty at 150 s averaging time

Nils Nemitz[1], Takuya Ohkubo[1,2,3], Masao Takamoto[1,2,4], Ichiro Ushijima[1,2,4], Manoj Das[1,2,4], Noriaki Ohmae[1,2,3] and Hidetoshi Katori[1,2,3,4*]

[1]Quantum Metrology Laboratory, RIKEN, Wako, Saitama 351-0198, Japan.

[2]Innovative Space-Time Project, ERATO, Japan Science and Technology Agency, Bunkyo-ku, Tokyo 113-8656, Japan.

[3]Department of Applied Physics, Graduate School of Engineering, The University of Tokyo, Bunkyo-ku, Tokyo 113-8656, Japan.

[4]RIKEN Center for Advanced Photonics, Wako, Saitama 351-0198, Japan.

* email: katori@amo.t.u-tokyo.ac.jp

Transition frequencies of atoms and ions are among the most accurately accessible quantities in nature, playing important roles in pushing the frontiers of science by testing fundamental laws of physics, in addition to a wide range of applications such as satellite navigation systems. Atomic clocks based on optical transitions approach uncertainties of 10^{-18} (ref. 1-3), where full frequency descriptions are far beyond the reach of the SI second. Direct measurements of the frequency ratios of such super clocks, on the other hand, are not subject to this limitation[4-8]. They can verify consistency and overall accuracy for an ensemble of super clocks, an essential step towards a redefinition of the second[9]. Here we report a measurement that finds the frequency ratio of neutral ytterbium and strontium clocks to be $\mathcal{R}$ = 1.207 507 039 343 337 749(55), with a fractional uncertainty of 4.6×10^{-17} and a measurement instability as low as 4×10^{-16} $(\tau/\text{s})^{-1/2}$.

This high stability marks a 90-fold reduction in the required averaging time over a previous record-setting experiment[4] that determined the ratio of Al^+ and Hg^+ single-ion clocks to an uncertainty of 5.2×10^{-17}. Enabled by the simultaneous interrogation of hundreds of atoms in optical lattice clocks[10], such a highly stable ratio measurement provides a powerful probe for new physics by exploring the variation $\Delta\alpha/\alpha$ of the fine structure constant with an uncertainty reducing as 1.6×10^{-15} $(\tau/\text{s})^{-1/2}$ (see

Methods). This already improves on dedicated experiments using atomic dysprosium[11] in a search for variations on a timescale of seconds[12], motivated by a coupling of light bosonic dark matter[13] to the electromagnetic field.

While the excitation of an atomic transition is described by a coherent quantum evolution, the readout of the outcome finds atoms in either the ground state or the excited state, introducing quantum projection noise[14] (QPN), which sets a quantum limit on clock stability that scales with atom number as $1/\sqrt{N}$. Consequently, optical lattice clocks operating with $N \gg 1$ offer a substantial advantage over single-ion clocks. Fully exploiting this excellent quantum-limited stability for a stand-alone clock relies crucially on the continued development of ultrastable clock lasers[15], since the noise of the local oscillator in conjunction with the periodic interrogation of the clock transition degrades stability through the Dick effect[16]. This, however, can be rejected in a synchronous comparison of two clocks[17,18], where shared frequency noise of the clock lasers leads to common Dick effect noise in the frequency evaluations, which can be cancelled out in determining the frequency ratio. An extension to this scheme promises interrogation times beyond the coherence time of the lasers[19]. Combining long interrogation times with increased atom numbers, synchronous comparisons of future optical lattice clocks may achieve a statistical uncertainty of 1×10^{-18} within minutes of averaging time[18]. This will
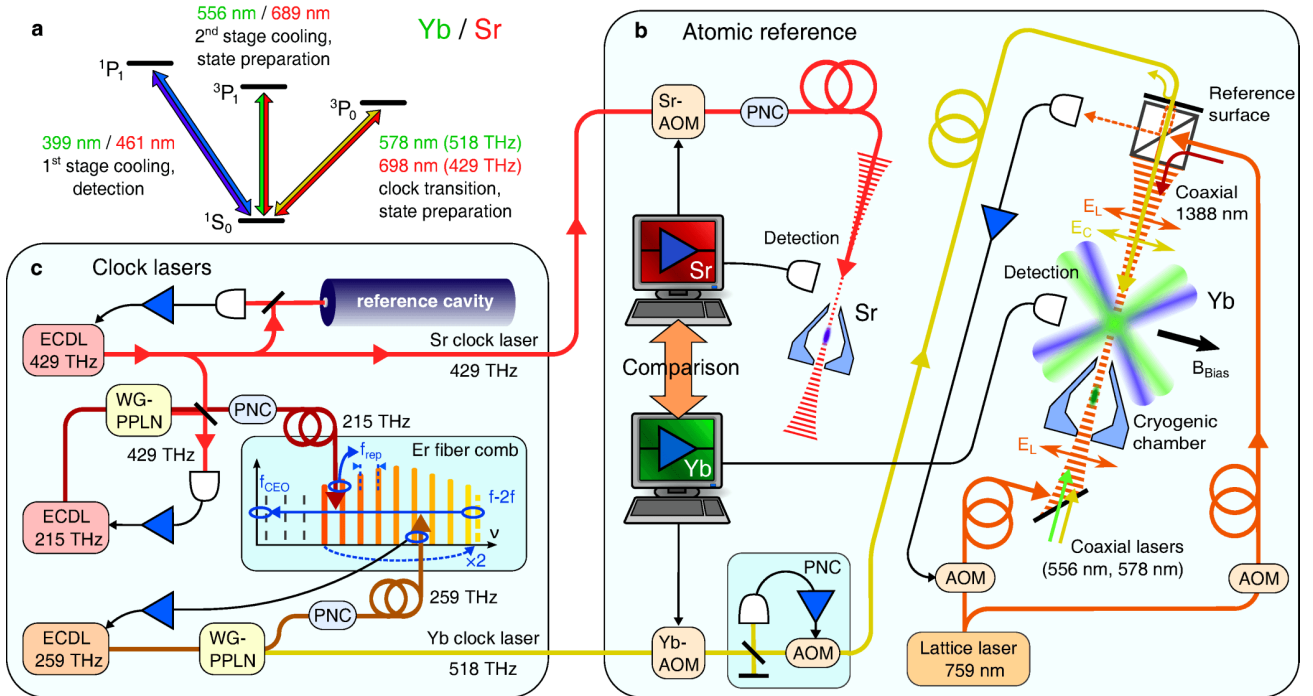
Figure 1 | Experimental setup of Yb/Sr ratio measurement. a, Relevant transitions in Yb and Sr. **b,** Optical scheme of Yb and Sr clocks. The control systems apply frequency corrections through acousto-optic modulators (AOM). PNC: phase-noise canceller. **c,** Generation of phase-locked clock lasers at $\nu_{Sr}^{cl} \approx 429$ THz and $\nu_{Yb}^{cl} \approx 518$ THz using an Er-fibre comb bridging the frequencies ν_{Sr}^{cl} / 2 and ν_{Yb}^{cl} / 2. Waveguide periodically-poled lithium niobate crystals (WG-PPLN) double the output frequencies of intermediary external-cavity diode lasers (ECDL).

allow instant investigation not only of clock frequency ratios, but also of relativistic effects equivalent to elevation changes of a single centimetre.

We apply synchronous interrogation in determining the ratio of the clock transition frequencies $v_{Yb} \approx 518$ THz and $v_{Sr} \approx 429$ THz in neutral ^{171}Yb and ^{87}Sr using a pair of cryogenic optical lattice clocks[2], designed for operation with either of the two atomic species. Figure 1 gives an overview of the experimental setup. Laser-cooled atoms loaded into the optical lattice are spin-polarized to more than 95% purity and sideband-cooled (see Methods and Supplementary Fig. 1) to an average axial vibrational state of $\bar{n} < 0.1$. We then probe the clock transitions using ultrastable clock lasers phase-locked through an optical frequency comb, as discussed below.

For clocks interrogating neutral Yb or Sr in a room temperature environment, the largest systematic frequency shift results from the AC Stark effect caused by blackbody radiation (BBR) and significant efforts have been made to control and characterize this effect[20-22]. In our experiments, the atoms are transported to a cryogenic chamber for interrogation. This shields the atoms from ambient BBR and results in a near hundred-fold reduction of the frequency shift; for Yb from -1.278 Hz at 300 K to $-14.2(4)$ mHz at 96 K, and for Sr from -2.278 Hz at 300 K to $-23.3(4)$ mHz at 95 K.

With less than 10^{-18} uncertainty of the BBR shifts, the largest uncertainty contribution for the ratio measurement stems from the lattice light shifts in the Yb clock. Taking into account atomic hyperpolarizability[23] and multipolar effects, the light shifts are modelled based on ref. 24 (see Methods and Supplementary Fig. 2 for details). We find $v_{E1} = 394,798,265(9)$ MHz for the E1-magic frequency, where the electric dipole polarizabilities of ground and excited states of the clock transition are equal.

We typically operate the optical lattice at $v_{op} = 394,798,278$ MHz, where the sensitivity to a variation of the lattice intensity is reduced by a partial cancelation of the linear and quadratic terms of the lattice-induced clock frequency shifts. For a typical trap depth $U_0 = 100\ E_r$ (≈ 10 μK), where E_r is the lattice photon recoil energy, our light shift model predicts a residual shift of $\Delta v_{ls} / v_{Yb} = (-12 \pm 32) \times 10^{-18}$. The uncertainty is dominated by the determination of the model parameters, but also accounts for deviations from ideal lattice conditions, as might result from an intensity imbalance or a spectrally broad background in the laser emission (see Methods). The uncertainty budgets for the two clocks and the ratio measurement are given in Table 1.

The Sr clock laser is stabilized to a 40-cm-long cavity and shows an instability of $3-5 \times 10^{-16}$ at 1 s. Its spectral characteristics are transferred to the Yb clock laser by a tight phase-lock, using an Er-fibre frequency comb with servo bandwidths ≈ 1 MHz[25]. The control systems for Yb and Sr then independently adjust the laser frequencies through acousto-optic modulators (AOM). After applying an interrogation pulse to the atoms in the optical lattice, the number of atoms in the ground and excited

Table 1 | Corrections and uncertainty contributions

Systematic effect:	^{171}Yb		^{87}Sr	
	Correction (10^{-18})	Uncertainty (10^{-18})	Correction (10^{-18})	Uncertainty (10^{-18})
Quadratic Zeeman effect	67.7	9.8	117.0	1.0
BBR shift	27.5	0.7	54.2	0.9
Lattice light shift	8.5	32.8	3.5	3.4
Probe light shift	-0.8	3.2	0.09	0.05
Collisions	0.0	3.4	0.9	4.2
AOM chirp and switching	0.0	1.1	0.0	0.2
1st order Doppler effect	0.0	2.0	0.0	0.5
Servo error	0.8	1.1	1.9	1.6
Single clock total	**103.7**	**34.7**	**177.6**	**5.8**

Yb/Sr ratio:	Correction (10^{-18})	Uncertainty (10^{-18})
Yb systematic effects	103.7	34.7
Sr systematic effects	-177.6	5.8
Laser-to-laser link	0.0	5.4
Gravitational shift	-0.3	0.2
Statistical uncertainty	0.0	28.6
Total	**-74.2**	**45.6**

Values are given in fractional units of 10^{-18} and represent averages over the complete set of contributing ratio measurements. See ref. 2 and Methods for details. The stated statistical uncertainty represents the standard deviation of the individual ratio measurements. The corrected ratio relates to the uncorrected transition frequencies $\tilde{\nu}_{Yb}$ and $\tilde{\nu}_{Sr}$ as $\mathcal{R} = \tilde{\nu}_{Yb}(1+\Delta_{Yb}) / [\tilde{\nu}_{Sr}(1+\Delta_{Sr})] \approx (1+\Delta_{Yb}-\Delta_{Sr})\,\tilde{\nu}_{Yb}/\tilde{\nu}_{Sr}$, where Δ_{Yb} and Δ_{Sr} are the fractional corrections for each transition frequency.

clock states, N_g and N_e, are detected to determine the atomic excitation $P = N_e / (N_g+N_e)$, which is used to estimate the deviation of the laser frequency from the atomic resonance and to calculate the required frequency correction.

We operate both clocks with the same cycle time of 1.5 s and simultaneously apply interrogation pulses of 200 ms duration. As a result, the atomic excitation in both clocks acquires a correlated fluctuation, as indicated in Fig. 2(b). The resulting common-mode noise cancels[18] for the clock frequency ratio $\mathcal{R} = \nu_{Yb} / \nu_{Sr}$, which is directly extracted from the record of applied corrections and resulting atomic excitation.

Figure 2(a) shows the fractional statistical uncertainty of the measured ratio $\mathcal{R}$, which falls as quickly as 4×10^{-16} $(\tau/s)^{-1/2}$ and reaches 1×10^{-17} with an averaging time below 3000 s. This is fully competitive with the stabilities of single species comparisons[21,26] that employ state-of-the-art clock lasers with instabilities of $1-2\times10^{-16}$ at 1 s.

Judging from the evaluation of interleaved Yb measurements, we find the synchronous interrogation to yield a two times improvement in stability compared to a measurement with uncorrelated laser noise

of similar magnitude (see Methods). The results demonstrate the excess noise introduced by the comb-based phase-lock to be low enough to approach the QPN limit of $2\times10^{-16}\,(\tau/s)^{-1/2}$ for 500 Yb and 1000 Sr atoms to a factor of two. For $\tau = 150$ s, the instability has already fallen below the systematic uncertainty of 3.6×10^{-17}, such that the overall uncertainty of the ratio measurement reaches 4.8×10^{-17}.

Over a period of four months, we performed ten measurements that are used to determine the Yb/Sr frequency ratio (Fig. 3). Due to the good short-term stability, the reproducibility of the measurements is not limited by the available averaging time, but by the uncertainties of the corrections applied for experimental parameters that differ between repeated measurements. The observed variation, with a fractional standard deviation of $\sigma_{\mathcal{R}}/\mathcal{R} = 2.9\times10^{-17}$, is consistent with the systematic ratio uncertainty of 3.6×10^{-17}. The scatter of the results may however mask additional uncertainties in the measurement (possibly resulting from changes in the effective lattice intensity experienced by the atoms, affecting the light shift, see Methods). We conservatively include this possibility by evaluating the statistical uncertainty as $\sigma_{\mathcal{R}}/\mathcal{R}$, with no reduction according to the standard error of the mean. This naturally
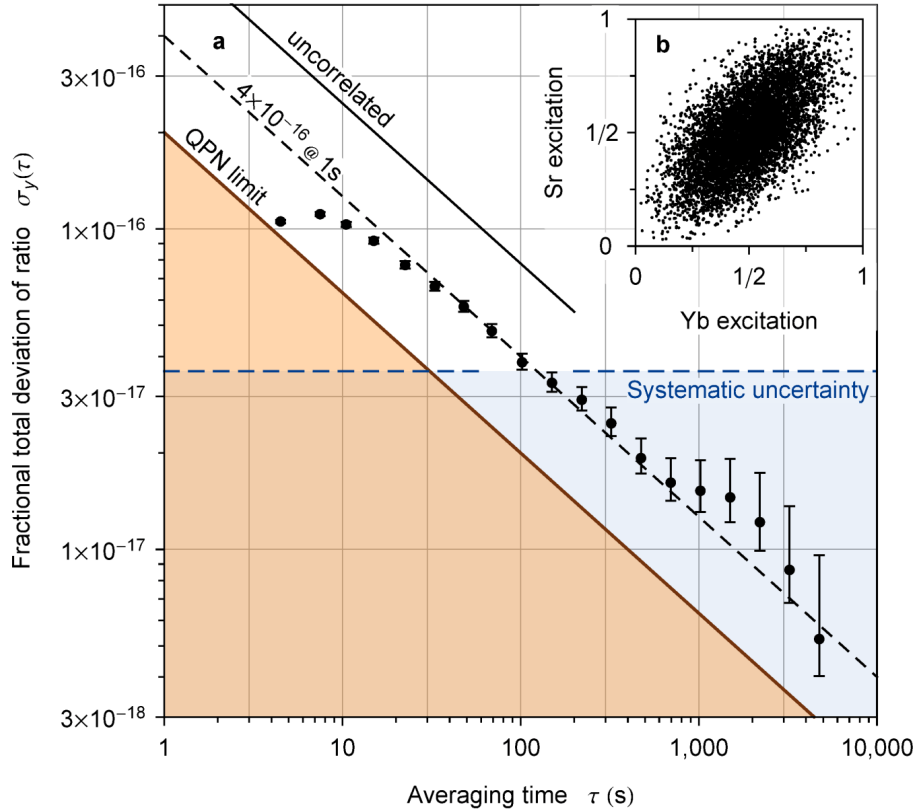
Figure 2 | Ratio measurement stability. a, The lowest observed short-term instability (given as fractional total deviation[29]), for a measurement of 10^4 s improves as $\sigma_y(\tau) = 4\times10^{-16}\,(\tau/s)^{-1/2}$ (black dashed line), approaching the QPN limit of $2\times10^{-16}\,(\tau/s)^{-1/2}$ for $N_{Yb} = 500$ and $N_{Sr} = 1000$ (brown line). Error bars indicate 1σ uncertainties, assuming white frequency noise. The stability estimated for an asynchronous measurement with similar but uncorrelated laser noise improves as $8\times10^{-16}\,(\tau/s)^{-1/2}$ (solid black line). Blue dashed line indicates the systematic ratio uncertainty of 3.6×10^{-17}. **b**, Correlation of atomic excitation detected in the Yb and Sr clocks after synchronous application of each clock pulse.

5
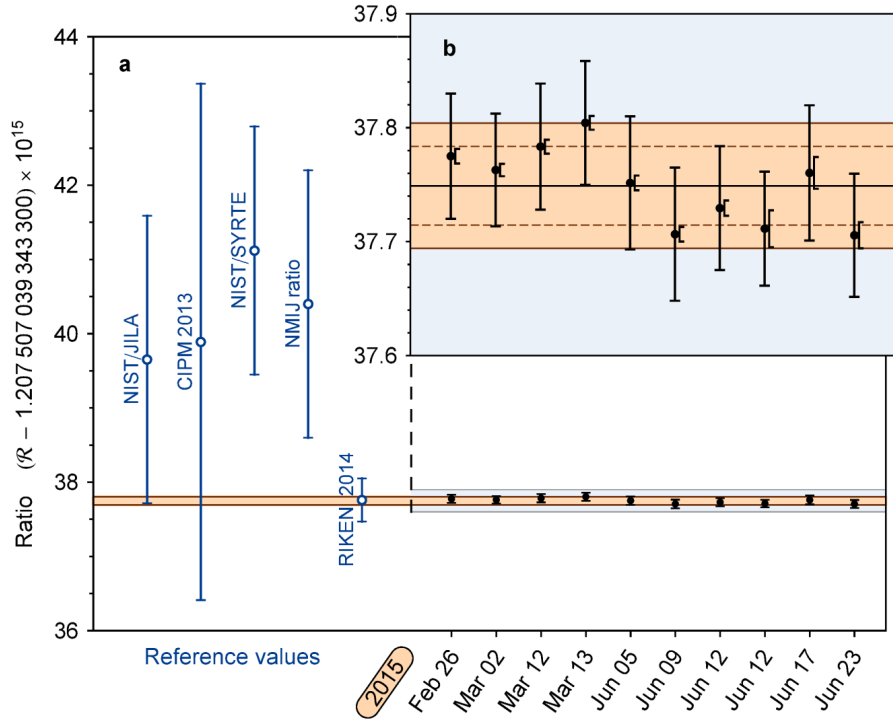
Figure 3 | History of ratio measurements. a, Orange shaded region marks the 1σ uncertainty of $\mathcal{R}$ as given in the text. Black circles show results of individual measurements, with indicated uncertainties combining systematic uncertainty and the statistical uncertainty obtained for the full data set. Ratios determined from previous measurements are shown in blue: "CIPM 2013" is calculated from the CIPM recommended frequencies[28], "NIST/JILA" from the frequency measurements with the lowest uncertainties listed therein, performed against the caesium standard at NIST. "NIST/SYRTE" compares the Yb measurement against more recent measurements of the Sr frequency[30]. "NMIJ ratio" results from a direct ratio measurement[7]. "RIKEN 2014" represents a measurement prior to those presented here[27]. **b,** Enlargement of blue-shaded region. Additional smaller error bars indicate statistical uncertainties obtained from the short-term stability of individual measurements, dashed lines show their standard deviation.

includes the smaller contribution resulting from the short-term instability. With equal weight assigned to each measurement, we find $\mathcal{R} = v_{Yb} / v_{Sr} = 1.207\ 507\ 039\ 343\ 337\ 749(43)_{sys}(35)_{stat}$, consistent with our prior measurement[27]. The fractional uncertainty of 4.6×10^{-17} represents a 30-fold reduction compared to a previous direct measurement at NMIJ[7], which yielded $\mathcal{R}^{NMIJ} = 1.207\ 507\ 039\ 343\ 340\ 4(18)$. Our value deviates from $\mathcal{R}^{NMIJ}$ by 1.5 times their stated uncertainty, but is well within the uncertainty of the ratio $\mathcal{R}^{CIPM} = 1.207\ 507\ 039\ 343\ 339\ 9(35)$ calculated from the transition frequencies recommended by the International Committee for Weights and Measures (CIPM)[28] in 2013.

Our ratio measurement obtains an overall uncertainty that improves on the best reported value. With enhanced control of the systematic effects, the measurement stability promises a statistical uncertainty of 1×10^{-18} with less than two days of averaging time. Operation with larger atom numbers will further relax the QPN limit and -together with improvements to clock laser stability- allow additional reductions in averaging times, making ratio measurements between optical lattice clocks a valuable tool in a search for new physics[11-13] at short time scales.

6

References

1. Chou, C. W., Hume, D. B., Koelemeij, J. C. J., Wineland, D. J. & Rosenband, T. Frequency comparison of two high-accuracy Al^+ optical clocks. *Phys. Rev. Lett.* **104,** 070802 (2010).

2. Ushijima, I., Takamoto, M., Das, M., Ohkubo, T. & Katori, H. Cryogenic optical lattice clocks. *Nature Photon.* **9,** 185-189 (2015).

3. Nicholson T. L. *et al.* Systematic evaluation of an atomic clock at 2×10^{-18} total uncertainty. *Nature Commun.* **6,** 6896 (2015).

4. Rosenband, T. *et al.* Frequency ratio of Al^+ and Hg^+ single-ion optical clocks; Metrology at the 17th decimal place. *Science* **319,** 1808-1812 (2008).

5. Matsubara, K. *et al.* Direct comparison of a Ca^+ single-ion clock against a Sr lattice clock to verify the absolute frequency measurement. *Opt. Express* **20,** 22034-22041 (2012).

6. Godun, R. M. *et al.* Frequency ratio of two optical clock transitions in $^{171}Yb^+$ and constraints on the time variation of fundamental constants. *Phys. Rev. Lett.* **113,** 210801 (2014).

7. Akamatsu, D. *et al.* Frequency ratio measurement of ^{171}Yb and ^{87}Sr optical lattice clocks. *Opt. Express* **22,** 7898-7905 (2014).

8. Yamanaka, K., Ohmae, N., Ushijima, I., Takamoto, M. & Katori, H. Frequency ratio of ^{199}Hg and ^{87}Sr optical lattice clocks beyond the SI limit. *Phys. Rev. Lett.* **114,** 230801 (2015).

9. Riehle, F. Towards a redefinition of the second based on optical atomic clocks. *C. R. Physique* **16,** 506-515 (2015).

10. Katori, H., Takamoto, M., Pal'chikov, V.G. & Ovsiannikov, V.D. Ultrastable optical clock with neutral atoms in an engineered light shift trap. *Phys. Rev. Lett.* **91,** 173005 (2003).

11. Van Tilburg, K., Leefer, N., Bougas, L. & Budker, D. Search for ultralight scalar dark matter with atomic spectroscopy. *Phys. Rev. Lett.* **115,** 011802 (2015).

12. Derevianko, A. & Pospelov, M. Hunting for topological dark matter with atomic clocks. *Nature Phys.* **10,** 933–936 (2014).

13. Schive, H., Chiueh, T. & Broadhurst T. Cosmic structure as the quantum interference of a coherent dark wave. *Nature Phys.* **10,** 496-499 (2014).

14. Itano, W. M. *et al.* Quantum projection noise: population fluctuations in two-level systems. *Phys. Rev. A* **47,** 3554-3570 (1993).

15. Häfner, S. *et al.* 8×10^{-17} fractional laser frequency instability with a long room-temperature cavity. *Opt. Lett.* **40,** 2112-2115 (2015).

16. Dick, G. J. Local oscillator induced instabilities in trapped ion frequency standards. In *Proceedings of 19th Precise Time and Time Interval Meeting, Redendo Beach, 1987*, 133-147 (U.S. Naval Observatory, Washington, DC, 1988).

17. Bize, S., Sortais, Y. & Lemonde, P. Interrogation oscillator noise rejection in the comparison of atomic fountains. *IEEE Trans. Ultrason. Ferroelectr. Freq. Control* **47,** 1253-1255 (2000).

18. Takamoto, M., Takano, T. & Katori, H. Frequency comparison of optical lattice clocks beyond the Dick limit. *Nature Photon.* **5,** 288-292 (2011).

19. Chou, C. W., Hume, D. B., Thorpe, M. J., Wineland, D. J. & Rosenband, T. Quantum coherence between two atoms beyond $Q=10^{15}$. *Phys. Rev. Lett.* **106,** 160801 (2011).

20. Middelmann, T., Falke, S., Lisdat, C. & Sterr U. High accuracy correction of blackbody radiation shift in an optical lattice clock. *Phys. Rev. Lett.* **109,** 263004 (2012).

21. Bloom, B. J. *et al.* An optical lattice clock with accuracy and stability at the 10^{-18} level. *Nature* **506,** 71-75 (2014).

22. Beloy, K. *et al.* Atomic clock with 1×10^{-18} room-temperature blackbody Stark uncertainty. *Phys. Rev. Lett.* **113,** 260801 (2014).

23. Barber, Z. W. *et al.* Optical lattice induced light shifts in an Yb atomic clock. *Phys. Rev. Lett.* **100,** 103002 (2008).

24. Katori, H., Ovsiannikov, V. D., Marmo, S. I. & Palchikov, V. G. Strategies for reducing the light shift in atomic clocks. *Phys. Rev. A* **91,** 052503 (2015).

25. Inaba, H. *et al.* Spectroscopy of ^{171}Yb in an optical lattice based on laser linewidth transfer using a narrow linewidth frequency comb. *Opt. Express* **21,** 7891-7896 (2013).

26. Hinkley, N. *et al.* An atomic clock with 10^{-18} instability. *Science* **341**, 1215-1218 (2013).

27. Takamoto, M. *et al.* Frequency ratios of Sr, Yb, and Hg based optical lattice clocks and their applications. *C. R. Physique* **16,** 489-498 (2015).

28. "Updates to the list of standard frequencies" CIPM Recommendation 1 (CI-2013). Available at http://www.bipm.org/en/publications/mises-en-pratique/standard-frequencies.html (2013).

29. Greenhall, C. A., Howe, D. A. & Percival, D. B. Total Variance, an estimator of long-term frequency stability. *IEEE Trans. Ultrason. Ferroelectr. Freq. Control* **46,** 1183-1191 (1999).

30. Le Targat, R. *et al.* Experimental realization of an optical second with strontium lattice clocks. *Nature Commun.* **4,** 2109 (2013).

31. Ma, L.-S., Jungner, P., Ye, J. & Hall, J. L. Delivering the same optical frequency at two places: accurate cancellation of phase noise introduced by an optical fiber or other time-varying path. *Opt. Lett.* **19,** 1777-1779 (1994).

32. Takamoto, M. et al. Improved frequency measurement of a one-dimensional optical lattice clock with a spin-polarized fermionic ^{87}Sr isotope. *J. Phys. Soc. Jpn.* **75,** 104302 (2006).

33. Angstmann, E. J., Dzuba, V. A. & Flambaum, V. V. Relativistic effects in two valence-electron atoms and ions and the search for variation of the fine-structure constant. *Phys. Rev. A* **70,** 014102 (2004).

34. Lea, S. N. Limits to time variation of fundamental constants from comparisons of atomic frequency standards. *Eur. Phys. J. Special Topics* **163,** 37–53 (2008).

35. Huntemann, N. *et al.* Improved limit on a temporal variation of m_p/m_e from comparisons of Yb$^+$ and Cs atomic clocks. *Phys. Rev. Lett.* **113,** 210802 (2014).

36. Uzan, J.-P. The fundamental constants and their variation: observational and theoretical status. *Rev. Mod. Phys.* **75,** 403-455 (2003).

37. Arvanitaki, A., Huang, J. & Van Tilburg, K. Searching for dilaton dark matter with atomic clocks. *Phys. Rev. D* **91,** 015015 (2015).

38. Falke, S. *et al.* A strontium lattice clock with 3×10^{-17} inaccuracy and its frequency. *New J. Phys.* **16,** 073023 (2014).

39. Santarelli, G. *et al.* Frequency stability degradation of an oscillator slaved to a periodically interrogated atomic resonator. *IEEE Trans. Ultrason. Ferroelectr. Freq. Control* **45,** 887-894 (1998).

40. Lemke, N. D. *et al.* Spin-1/2 optical lattice clock. *Phys. Rev. Lett.* **103,** 063001 (2009).

41. Sherman, J. A. *et al.* High-accuracy measurement of atomic polarizability in an optical lattice clock. *Phys. Rev. Lett.* **108,** 153002 (2012).

42. Blatt, S. *et al.* Rabi spectroscopy and excitation inhomogeneity in a one-dimensional optical lattice clock. *Phys. Rev.* A 80, 052703 (2009).

43. Ovsiannikov, V. D., Pal'chikov, V. G., Taichenachev, A. V., Yudin, V. I. & Katori, H. Multipole, nonlinear, and anharmonic uncertainties of Sr atoms in an optical lattice. *Phys. Rev. A* **88,** 013405 (2013).

44. Lemke, N. D. *et al.* p-wave cold collisions in an optical lattice clock. *Phys. Rev. Lett.* **107,** 103902 (2011).

45. Falke, S., Misera, M., Sterr, U. & Lisdat, C. Delivering pulsed and phase stable light to atoms of an optical clock. *Appl. Phys. B* **107,** 301-311 (2012).

46. Iwakuni, K. *et al.* Narrow linewidth comb realized with a mode-locked fiber laser using an intra-cavity waveguide electro-optic modulator for high-speed control. *Opt. Express* **20,** 13769-13776 (2012).

Author contributions
H.K. initiated and coordinated the experiments. M.T. and I.U. characterized and operated the Sr clock, N.N. and T.O. the Yb clock. N.O. maintained and operated the frequency comb. All authors contributed to the experimental setups, discussed the results and commented on the manuscript.

Methods

Operation of the Yb clock

Fermionic ^{171}Yb $\left(I = \frac{1}{2}\right)$ atoms are decelerated from a thermal beam that contains both Sr and Yb atoms by a Zeeman slower and trapped in a magneto-optical trap (MOT), operating on the $^1S_0 - {}^1P_1$ transition at 399 nm. A second cooling stage in a MOT on the $^1S_0 - {}^3P_1$ transition at 556 nm reduces the atomic temperature to 15 μK. The optical lattice is kept at full intensity during loading. It provides a trap depth $U_0 / k_B \approx 10$ μK or $U_0 \approx 100 \, E_r$, with the lattice photon recoil energy $E_r = (h / \lambda_L)^2 / (2 \, m)$, where $\lambda_L \approx 759$ nm is the lattice laser wavelength, and m is the atomic mass.

Around 500 atoms at a temperature of 3 μK remain in the lattice after turning off the MOT beams. Changing the frequency of one of the two independent lattice beams creates a moving lattice, which

transports the atoms by a chosen distance of typically 18−20 mm into the cryogenic chamber located below the MOT region (see Fig. 1). Outside of the 60 ms transport interval, the relative phase of the lattice beams is actively stabilized to fix the lattice anti-nodes relative to a reference mirror[2].

To interact with the atoms inside the cryogenic chamber, additional coaxial laser beams (see Fig. 1b) are superimposed on the optical lattice with the same linear polarization. Spin-polarization is realized by optical pumping on the $^1S_0 \left(F = \frac{1}{2}\right) - {}^3P_1 \left(F = \frac{3}{2}\right)$ transition, where a bias magnetic field of 70 µT separates the Zeeman components by 900 kHz and allows the $\pi-$transitions ($m_F = \pm \frac{1}{2}$ to $m_F = \pm \frac{1}{2}$) to be independently addressed. Two additional beams are used for axial sideband cooling: The first beam excites the red sideband of the $^1S_0 - {}^3P_0$ clock transition at 578 nm with a Rabi frequency of $\Omega_R^{red} > 2\pi \times 100$ Hz. The second beam is resonant with the $^3P_0 \left(F = \frac{1}{2}\right) - {}^3D_1 \left(F = \frac{1}{2}\right)$ transition at 1388 nm and returns the atoms to the ground state. Simultaneous operation of all three beams accumulates spin-polarized atoms in the dark $n = 0$ axial vibrational state over a period of 100 ms (see
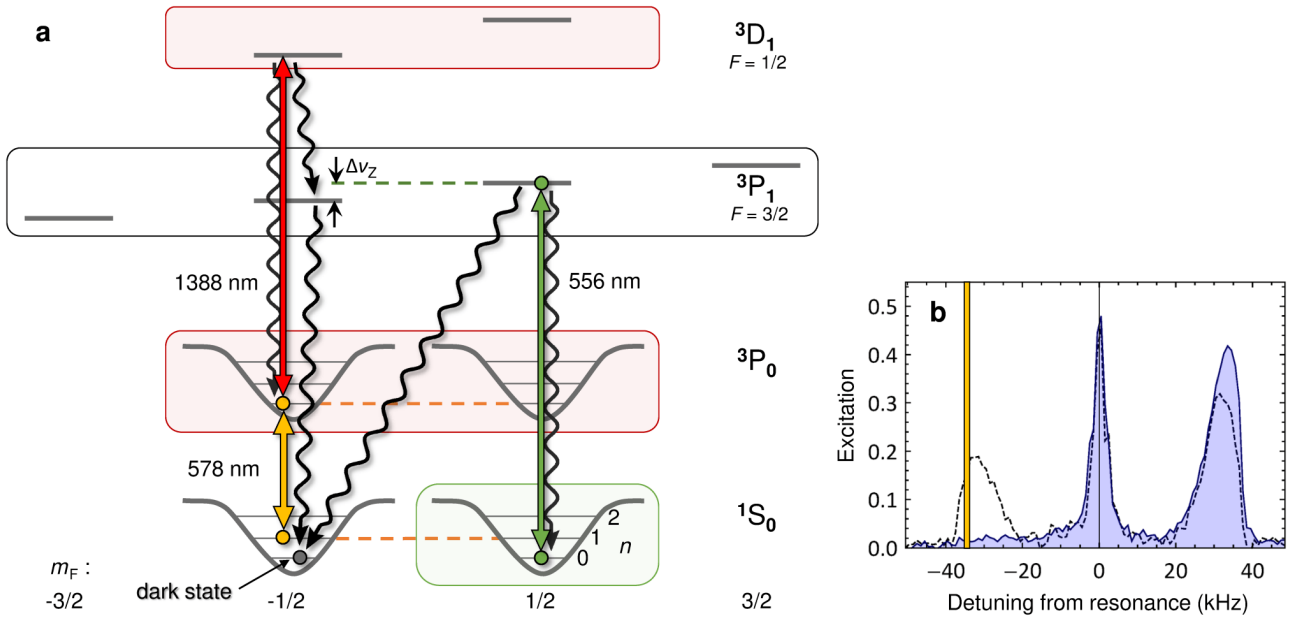
Supplementary Figure 1 | Yb state preparation. a, Relevant excitation and decay paths. Coloured areas indicate manifolds of substates addressed by the respective laser. Atoms are excited from an axial vibrational state n in $^1S_0$ ($m_F = \pm \frac{1}{2}$) to $n - 1$ in $^3P_0$ ($m_F = \pm \frac{1}{2}$) by a laser tuned near the edge of the red sideband of the clock transition at 578 nm. The resulting population in the $^3P_0$ state is excited to the short-lived $^3D_1$ ($F = \frac{1}{2}$) state, which provides a decay path to the ground state via $^3P_1$. While the vibrational state is not resolved for the $^1S_0$ to $^3P_1$ transition, the Zeeman splitting $\Delta\nu_Z$ of the $^3P_1$ ($F = \frac{3}{2}$) state allows for spin-polarization to $m_F = -\frac{1}{2}$ [$m_F = \frac{1}{2}$] by exciting the $m_F = \frac{1}{2}$ to $m_F = \frac{1}{2}$ [$m_F = -\frac{1}{2}$ to $m_F = -\frac{1}{2}$] component. While the atoms may return to the $m_F = \frac{1}{2}$ substate or to a vibrational state $n > 0$ via alternative decay paths (not shown), they gradually accumulate in the dark state with $n = 0$ in $^1S_0$ ($m_F = -\frac{1}{2}$). **b,** Sideband spectrum showing a reduction of the average axial vibrational state from $\bar{n} = 0.7$ without sideband cooling (dashed line) to $\bar{n} \approx 0.04$ with sideband cooling (solid, blue shaded curve). The vertical orange line marks a typical frequency of the sideband cooling laser.

Supplementary Fig. 1). We typically find >95% of atoms in the desired spin state and an average axial vibrational quantum number $\bar{n} \approx 0.08$.

A Rabi interrogation pulse of 200 ms is applied using a separate 578 nm beam (see Fig. 1b), which is phase-stabilized[31] to the same reference surface as the lattice. After interrogation, the atoms are transported back to the loading region by the moving lattice and a sequence of three camera images is acquired to extract the atomic excitation from the background-corrected fluorescence signals of atoms in the ground and excited state. Over a 4-step sequence, the clock laser probes the left and right slopes of the $m_F = \pm\frac{1}{2}$ components to measure and correct for the clock laser drift while cancelling out the first order Zeeman shift and the vector Stark shift[32].

Sensitivity to changes in the fine structure constant

To the first order, the measured frequency ratio varies with α as $\Delta\mathcal{R}/\mathcal{R} = (A_{Yb} - A_{Sr})\,\Delta\alpha/\alpha$, where $A_{Yb} = 0.31$ and $A_{Sr} = 0.06$ are sensitivity factors for Yb and Sr[33,34]. Certain ion clocks, such as those using Hg^+ ($A_{Hg+} = -3.2$) or the octupole clock transition in Yb^+ ($A_{Yb+}^{oct} = -5.3$) exhibit larger sensitivities and offer a clear advantage in a search for a long term drift $\dot{\alpha}$ over a period of months or years[4,6,35,36]. When looking for a sudden change $\Delta\alpha$ associated with the passage of topological defect dark matter[12] or oscillations in its value induced by a coupling to ultralight dilaton dark matter[11,37], the longer averaging times required by ion clocks negate this advantage at least partially: For the Al^+/Hg^+ ratio[4], an instability of $3.9\times10^{-15}\,(\tau/s)^{-1/2}$ was reported, equivalent to a sensitivity to $\Delta\alpha/\alpha$ improving as $\sigma_y^\alpha(\tau) = 1.2\times10^{-15}\,(\tau/s)^{-1/2}$. For an Yb^+/Sr comparison[38] the reported instability was $5.3\times10^{-15}\,(\tau/s)^{-1/2}$, corresponding to $\sigma_y^\alpha(\tau) = 1.0\times10^{-15}\,(\tau/s)^{-1/2}$. In terms of the limit that can be set on $\Delta\alpha/\alpha$ for short averaging times, the sensitivity of $\sigma_y^\alpha(\tau) = 1.6\times10^{-15}\,(\tau/s)^{-1/2}$ for our Yb/Sr measurement is therefore already competitive with existing experiments. Further improvements are expected with increased atom number.

Ratio determination from recorded steering data

The control systems store the applied AOM frequencies $\Delta f_{Yb(Sr)}^{AO}$ and resulting atomic excitation P. The excitation is used to calculate the error signal δv, corresponding to the deviation of the applied clock laser frequency from the HWHM point of the Rabi lineshape.

The subharmonics of the clock laser frequencies, $v_{Sr}^{cl}/2$ and $v_{Yb}^{cl}/2$, are used to create beat signals with the comb lines with indices n_{Sr} and n_{Yb}. The clock frequency ratio $\mathcal{R} = v_{Yb}/v_{Sr}$ can be extracted from recorded data as

$$\mathcal{R} = r + \frac{(f_{CEO} + \Delta f_{Yb}^*/2) - r(f_{CEO} + \Delta f_{Sr}^*/2)}{n_{Sr}\,f_{rep} + (f_{CEO} + \Delta f_{Sr}^*/2)}, \qquad (1)$$

where $r = n_{Yb} / n_{Sr}$, and f_{rep} and f_{CEO} are the comb repetition rate and carrier-envelope offset frequency. The frequency offsets $\Delta f^*_{Yb(Sr)} = \Delta f^{AO}_{Yb(Sr)} - \Delta v^{step}_{Yb(Sr)} + \Delta f^{const}_{Yb(Sr)} + \Delta v^{cor}_{Yb(Sr)} - \delta v_{Yb(Sr)}$ include the AOM frequency $\Delta f^{AO}_{Yb(Sr)}$, corrected for the frequency step $\Delta v^{step}_{Yb(Sr)}$ applied to probe the left and right slopes of the two Zeeman components. All constant frequency offsets are included in $\Delta f^{const}_{Yb(Sr)}$, while $\Delta v^{cor}_{Yb(Sr)}$ corrects for systematic shifts. The division by two accounts for the use of the subharmonics. During a ratio measurement, f_{CEO} is stabilized to a reference frequency. Instead of directly measuring f_{rep}, we substitute $n_{Sr} f_{rep} + (f_{CEO} + \Delta f^*_{Sr}/2) = v_{Sr}/2$, which is known to a fractional uncertainty of less than 10^{-15}. A larger uncertainty is introduced by the instability of the radio-frequencies (RF), which are derived from a GPS-conditioned BVA quartz oscillator with an instability of $\leq 5 \times 10^{-12}$ for $\tau > 0.2$ s. However, both affect only the last term in equation (1), which is on the order of 10^{-7} with proper choice of the referenced comb lines, for a resulting uncertainty $<10^{-18}$, as discussed later.

Short-term stability during Yb/Sr comparisons and interleaved evaluation

In a simple model of the Dick effect contribution to the short-term stability based on ref. 39, we treat the Sr clock laser as dominated by cavity thermal noise, with a constant flicker FM instability of $\sigma_y(\tau) \approx 3 \times 10^{-16}$, and the link between clock lasers as a source of white phase noise chosen to reproduce $\sigma_y^{sync}(\tau) = 4 \times 10^{-16} (\tau/s)^{-1/2}$. The model predicts an instability of $1.4 \times 10^{-15} (\tau/s)^{-1/2}$ for an interleaved measurement in the Yb clock with a cycle time of 3 s, in agreement with experimental results under optimal conditions. For a comparison of Yb and Sr clocks with uncorrelated noise, the predicted instability for a cycle time of 1.5 s is $\sigma_y^{async}(\tau) = 8 \times 10^{-16} (\tau/s)^{-1/2}$, with contributions from individual clock instabilities of $\sigma_y^{Sr}(\tau) = 5 \times 10^{-16} (\tau/s)^{-1/2}$ and $\sigma_y^{Yb}(\tau) = 6 \times 10^{-16} (\tau/s)^{-1/2}$. The Yb/Sr comparison is well-suited to synchronous interrogation due to the similar clock frequencies[18], and further noise reduction in the phase-lock between the lasers will allow even greater stability.

Uncertainty budget of the Yb clock

The following sections discuss the uncertainty contributions stated in Table 1 for the Yb clock.

Quadratic Zeeman shift

The alternating interrogation of the $m_F = \pm\frac{1}{2}$ components provides a continuous measurement of the magnetic field. We use the coefficients reported in ref. 40 to correct for the resulting quadratic Zeeman shift.

BBR shift

A detailed study of the residual BBR frequency shifts for atoms inside the cryogenic chamber and their uncertainty was performed for Sr (ref. 2). As the contribution from the dynamic polarizability is insignificant at $T = 96$ K, the twice lower DC-polarizability of Yb compared to Sr leads to a further reduction of shift and uncertainty. Precise experimental polarizability coefficients are available in refs. 22,41.

As the lattice waist is located between the loading position and the entrance aperture of the cryogenic chamber, the trap depth falls with increased transport distance inside the chamber. To avoid excessive atom loss in the Yb clock, where the temperature of the trapped atoms is higher than for Sr, atoms are interrogated at a chosen position located 5-7 mm inside the chamber, as opposed to 9 mm for Sr. The increased effect of room-temperature BBR leaking into the chamber is included in the uncertainty contribution of 7×10^{-19}.
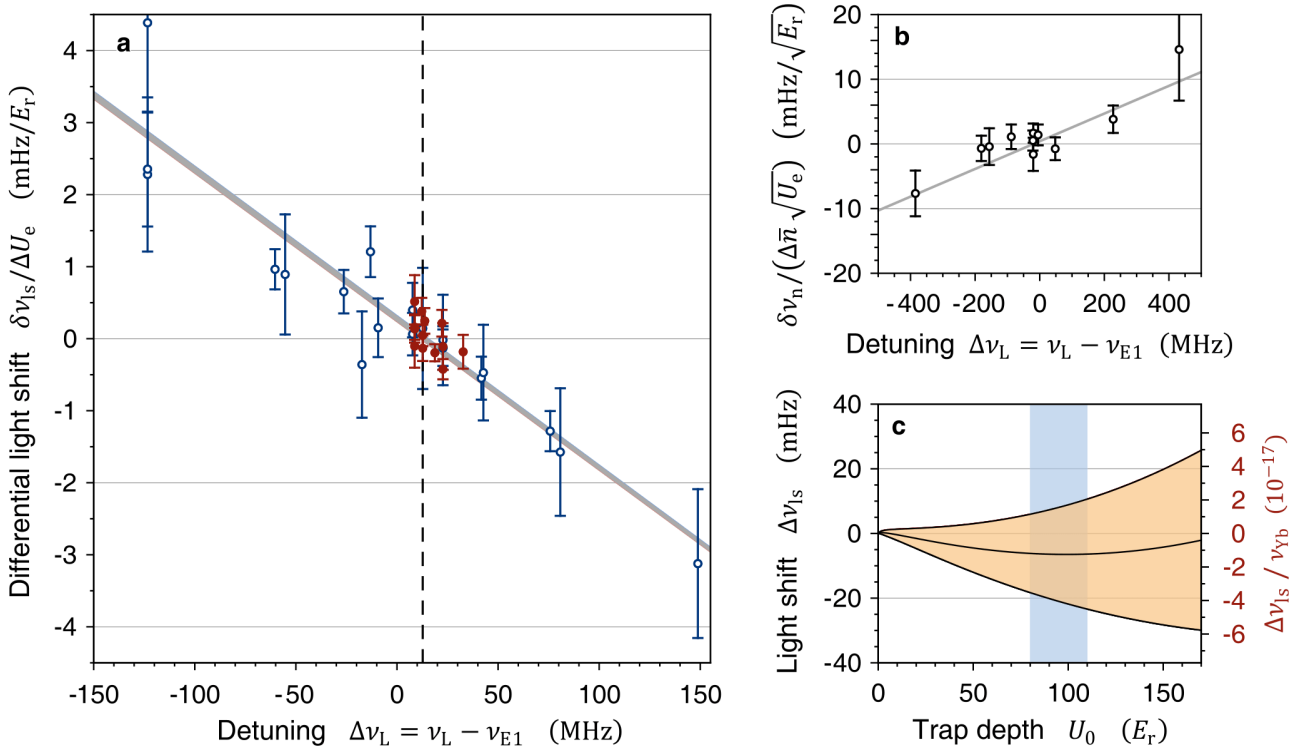
Lattice light shifts

In Yb, the presence of several allowed two-photon transitions close to the magic frequency introduces hyperpolarizability effects large enough to require consideration even at the 10^{-17} level[23]. The magnitude of the multipolar polarizability has also been studied only theoretically. To include both effects in our evaluation, we model the lattice-induced light shift $\Delta\nu_{ls}$ as

$$\Delta\nu_{ls} = (a\,\Delta\nu_L - b)\left(\bar{n} + \tfrac{1}{2}\right)\sqrt{U_e/E_r} - \left(a\,\Delta\nu_L + \tfrac{3}{4}d\,(2\bar{n}^2 + 2\bar{n} + 1)\right)U_e/E_r$$
$$+ d(2\bar{n} + 1)(U_e/E_r)^{3/2} - d(U_e/E_r)^2 , \qquad (2)$$

derived from equation (12) of ref. 24 by substituting the single beam intensity $I = U_e/\alpha_{E1}$, where the atomic electric dipole (E1) polarizability α_{E1} is identical for ground and excited clock states at the E1-magic frequency ν_{E1}. The equivalent axial trap depth $U_e = \zeta\,U_0$ represents the reduced intensity experienced by the atoms due to their radial motion[8]. The coefficient a describes the slope of the differential E1-polarizability at ν_{E1}, while the coefficients b and d correspond to the combined multipolar polarizability and hyperpolarizability, respectively. $\Delta\nu_L = \nu_L - \nu_{E1}$ is the detuning of the lattice frequency ν_L from ν_{E1}. Replacing the individual atomic axial vibrational quantum number n by the ensemble average $\bar{n}$ is a convenient approximation for our experiments, where $\bar{n} < 1$. The parameters U_0, ζ and $\bar{n}$ are extracted from axial sideband spectra for each measurement using methods based on ref. 42. For the hyperpolarizability coefficient we adopt a value of $d = -1.9(8)$ μHz to reproduce the results of ref. 23. The increased uncertainty results mainly from our estimation of $\zeta_{NIST} = 0.70(14)$.

To find a, b and ν_{E1}, the light shift model is simultaneously fitted to the data accumulated in 50 interleaved measurements, varying either the trap depth or –by alternating between operation with and without sideband cooling– the vibrational state (see Supplementary Fig. 1 and 2). When determining the weighting for this fit, we consider the uncertainties of the determined parameters, particularly the equivalent trap depth U_e, in addition to the statistical uncertainty of the measurement itself. This avoids introducing errors by putting excessive weight on individual measurements that depend critically on these input parameters, such as light shift measurements far detuned from the magic frequency. All statistical uncertainties are inflated by $\sqrt{\chi^2} = 1.2$ based on a subset of 29 measurements within 100 MHz of the magic frequency, where the parameter dependence is small compared to the statistical uncertainty of a single measurement.

Supplementary Figure 2 | Characterization of lattice light shifts. a, Measured differential frequency shift $\delta\nu_{ls}$ with change of equivalent trap depth $U_e = \zeta\,U_0$ as function of lattice detuning $\Delta\nu_L$ from $\nu_{E1} = 394{,}798{,}265$ MHz. Blue open circles indicate measurements alternating between $U_0^{hi} \approx 100\,E_r$ and $U_0^{lo} \approx 70\,E_r$ inside the cryogenic chamber. Red full circles indicate measurements outside the chamber, where proximity to the beam waist allows alternation between $U_0^{hi} \approx 160\,E_r$ and $U_0^{lo} \approx 90\,E_r$. Error bars show 1σ statistical uncertainties after inflation for excess scatter as discussed in the text. The grey line indicates the prediction of the light shift model, its width covers typical parameters for both types of measurements. Additional measurements (not shown) were taken at $|\Delta\nu_L| \geq 1\,\mathrm{GHz}$ to accurately determine the detuning dependence of the light shift. Vertical dashed line marks the operating point ν_{op}. **b,** Frequency shift with change of average axial vibrational state $\bar{n}$, plotted as $\delta\nu_n/(\Delta\bar{n}\sqrt{U_e})$ for normalization. Error bars give inflated statistical uncertainties and the grey line shows the prediction for a measurement alternating between typical values of $\bar{n}^{hi} = 0.8$ and $\bar{n}^{lo} = 0.08$ for $U_0 = 100$ to $160\,E_r$. **c,** Estimated light shift and uncertainty of the model as function of trap depth U_0 for $\nu_L = \nu_{op} = 394{,}798{,}278$ MHz, blue shaded region indicates the range of U_0 typical for our experiments.

14

The uncertainties of the coefficients extracted from the fit represent uncertainties uncorrelated between measurements. To take into account systematic errors that are shared between measurements, specifically in our determination of ζ and $\bar{n}$ from the sideband spectra and the adopted value of d, we employ a Monte-Carlo method for our data analysis. In this procedure, fitting is repeated for different permutations of these parameters and the RMS deviation of the obtained coefficients is added to their uncertainties in quadrature. The effects of collisional shifts on the light shift evaluation are also included at this stage.

Overall, we find $a = 0.021(6)$ mHz/MHz and $b = -0.68(71)$ mHz, as well as $\nu_{\mathrm{E1}} = 394{,}798{,}265(9)$ MHz. Typical parameter values are $\zeta = 0.72(5)$ and $\bar{n} = 0.08(8)$ when sideband cooling is applied.

Lattice light impurity

The optical lattice is generated by the output of a Ti:Sapphire laser, filtered with a volume Bragg grating (VBG) with a FWHM of 40 GHz. The lattice frequency is determined to within 200 kHz using the frequency comb. The optical spectrum shows no amplified spontaneous emission above the noise floor of the spectrum analyser, and a monitoring Fabry-Pérot etalon shows no spurious frequency components during normal operation.

Although we do not expect a frequency shift, we perform a check by deliberately detuning the centre frequency of the VBG by $f_{\mathrm{rel}}^{\mathrm{VBG}} = \pm 10$ GHz from the lattice laser frequency ν_{L} to impose an asymmetric shape on a possible spectrally broad background. We then measure the light shift by varying the lattice intensity. Extrapolated to a trap depth of $U_0 = 100\,E_{\mathrm{r}}$, the results correspond to a fractional frequency shift of $(\Delta\nu_{\mathrm{bg}} / \nu_{\mathrm{Yb}}) / \Delta f_{\mathrm{rel}}^{\mathrm{VBG}} = -1.9(1.4)\times10^{-18}$/GHz. For an alignment of the VBG centre-frequency according to $f_{\mathrm{rel}}^{\mathrm{VBG}} = 0(5)$ GHz in normal operation, we include a fractional uncertainty of 1.2×10^{-17} (at $100\,E_{\mathrm{r}}$) in the lattice light shift uncertainty.

Running wave frequency shifts

The multipolar polarizability assumed in our light shift model contributes a frequency shift of $\Delta\nu_{\mathrm{mp}} / \nu_{\mathrm{Yb}} \approx -b(\bar{n} + 1/2)\sqrt{U_{\mathrm{e}}/E_{\mathrm{r}}} = 6.4(6.8)\times10^{-18}$ for nominal trapping parameters (equation (2)). This shift varies with the shape of the trapping potential, with the model assuming a pure standing-wave field. An imbalance in lattice beam intensity creates an admixture of running-wave field that may cause a frequency shift[43] $\Delta\nu_{\mathrm{rw}}$.

To investigate the effect, a measurement is performed near the beam waist, where a trap depth of $U_0 = 165\,E_{\mathrm{r}}$ at full lattice intensity corresponds to a single beam peak intensity of $I = 10$ kW/cm^2.

Reducing the intensity of one lattice beam to $I_1 = 1.5$ kW/cm^2 results in a strong intensity imbalance $\Delta I = I_2 - I_1 = 8.5$ kW/cm^2. Interleaved measurements alternate between this imbalanced configuration and a balanced configuration with $I_1 = I_2 = 6$ kW/cm^2, corresponding to the intensity inside the cryogenic chamber. We find a statistically insignificant frequency shift of $\Delta\nu_{rw}/\nu_{Yb} = 1.4(2.8)\times10^{-17}$. For a linear model $\Delta\nu_{rw}/\nu_{Yb} = c_{rw}\,|\Delta I|$ with $c_{rw} = 1.6(3.3)\times10^{-18}/(\text{kW/cm}^2)$ the maximum expected imbalance of $\Delta I = 1.2$ kW/cm^2 then yields a frequency shift of $2.0(3.9)\times10^{-18}$. To avoid introducing an unwarranted frequency correction, we include this in the lattice light shift uncertainty budget as $0.0(5.9)\times10^{-18}$.

Probe light shift

The intensity required to apply a Rabi π-pulse over the interrogation time t_i falls as $I_{pr} \propto t_i^{-2}$, strongly reducing frequency shifts for longer interrogation times. We use the values reported in ref. 40, rescaled to $t_i = 200$ ms, to determine the probe light shift and its uncertainty.

Collisional shifts

For a typical atom number of $N_{Yb} = 500$, the average population per lattice site is less than one. We expect a suppression of p-wave collisions due to the low atomic temperature of 3 μK and trap depth equivalent to 10 μK, both significantly below the p-wave barrier of ≥ 30 μK[44]. In a spin-polarized and homogeneously excited sample, the Pauli exclusion principle prohibits s-wave collisions.

We investigate density-induced frequency shifts by measurements alternating between high and low atom numbers and observe no statistically significant effect over repeated measurements. For the lattice configuration inside the cryogenic chamber, a trap depth of $U_0 = 100\,E_r$ and $N_{Yb} = 500$, we adopt a fractional uncertainty of 4×10^{-18}. The Monte-Carlo stage of the light shift analysis also varies the collisional shift coefficient according to this uncertainty. To include the effect of density changes with trap depth, we apply a scaling according to $U_0^{3/2}$ (ref. 3).

First-order Doppler shift

The phase of the clock laser and the positions of the lattice antinodes are actively stabilized to the same reference surface[2]. We include an uncertainty of 0.5×10^{-18} to account for residual variations in the clock laser path length.

In our experiments, the lattice axis is oriented at a 15° angle from vertical, such that gravity causes a transverse displacement of the atomic distribution that varies with radial confinement. Changes in lattice intensity can therefore induce atomic motion during interrogation. This motion follows the wavefront of the lattice, and unless the wave-vector of the clock laser is perfectly perpendicular, will result in an additional Doppler shift. We investigate the effect by applying lattice intensity ramps

characterized by $\dot{U}_0 = dU_0/dt \approx \pm125\ E_r/$s during interrogation. The largest observed frequency shifts are equivalent to $(\Delta\nu_{\text{Dop}}/\nu_{\text{Yb}})\ /\ \dot{U}_0 \approx 2\times10^{-18}\ /\ (E_r/s)$.

The intensities of the lattice beams are not actively stabilized and persistent intensity changes correlated with the experimental cycle might be introduced by thermal effects in the lattice AOMs. However, even following an intensity reduction from 100% to 85% during the state preparation period, we observe intensity changes corresponding to only $\dot{U}_0 = 0.0(1.0)\ E_r/$s. We adopt an uncertainty of 1.9×10^{-18} due to induced transverse motion, for a total first-order Doppler-shift uncertainty of 2×10^{-18}.

AOM chirp and switching

The AOM used to apply frequency corrections to the clock laser is operated at an RF power of only 20 mW to reduce thermal effects. Instead of being switched off outside the interrogation time, the applied frequency is simply detuned by 100 kHz. At the beginning of the clock interrogation, the frequency switch to resonance causes a reproducible phase excursion of the phase-noise cancellation system. We calculate a resulting frequency shift of 3×10^{-19} (ref. 45). This is further suppressed by randomly alternating between positive and negative detuning, for which the phase excursion likewise changes in sign. A loop-back test confirms the absence of phase drift and chirp: An additional optical fibre returns the light sent to the experimental chamber back to the clock laser, where a partial mirror serves as phase reference. The beat with the unshifted clock laser light directly after the WG-PPLN (see Fig. 1) is then measured by a frequency counter gated to the interrogation time. We find no frequency deviation or instability larger than 1.1×10^{-18}, which we take as the uncertainty.

Servo error

Both control systems contain algorithms to determine and predict the drift of the clock lasers. For a combined dataset of all ratio measurements, we find that the mean in-loop error signal $\overline{\delta\nu}$, extracted from the detected atomic excitation, reaches $-0.8(1.1)\times10^{-18}$ for Yb and $-1.9(1.6)\times10^{-18}$ for Sr, where the instabilities have been determined from the Allan deviation.

The effect of the servo error on the measured frequency ratio is corrected shot-to-shot by including $\delta\nu$ in the Δf_{Yb}^* and Δf_{Sr}^* terms of equation (1). Based on the instability of $\overline{\delta\nu}$, we adopt uncertainty contributions from a long-term servo error of $\sigma_{\text{sv}}^{\text{Yb}} = 1.1\times10^{-18}$ and $\sigma_{\text{sv}}^{\text{Sr}} = 1.6\times10^{-18}$.

DC Stark shifts

During interrogation, the atoms are shielded from external electric fields by the copper construction of the cryogenic chamber. Although the inner surfaces are black-coated to suppress reflections of room-temperature BBR, a surface resistivity of $R_s < 2\times10^6\ \Omega\ /\ \square$ avoids the build-up of stray charges. We

therefore do not expect any significant DC Stark shift. This is supported by the results of experiments operating both clocks with Sr, which find agreement throughout the period spanned by the ratio measurements.

Additional uncertainties for ratio measurements

The following sections describe additional uncertainties in the comparison of the two clocks.

Laser-to-laser link uncertainty

The frequency comb was constructed at AIST/NMIJ, where the frequency stability of a near-identical comb was evaluated[46] as approximately 2.3×10^{-18} for $\tau = 10^3$ to 10^4 s and falling to below 10^{-18} for $\tau > 10^4$ s. Since we operate the comb in an environment temperature-controlled to 0.1 K, we expect similar stability.

Phase instabilities from variations in the optical path lengths between the clock lasers and the comb also contribute here. To avoid including the unstabilized lengths of the in-coupling fibres of the WG-PPLN systems, the stabilization of the comb repetition rate and the Yb clock laser use the residual fundamental light transmitted through the crystal, where the frequency doubling process ensures a stable phase relation with the generated harmonic output (Fig. 1). The fibres connecting the clock lasers to the comb are equipped with phase-noise cancellation systems[31]. Based on the stability of the loop-back measurements described above, which include a large fraction of the residual unstabilized optical path (approximately 2 m combined between Yb and Sr systems), we adopt an uncertainty of 2×10^{-18}.

The stability of the RF reference affects the ratio measurements through the last term of equation (1), particularly the reference frequencies for the beat signals used in the phase lock as well as the phase noise cancellation, entering through $\Delta f_{\text{Yb(Sr)}}^{\text{const}}$. For the first four measurements we include an uncertainty contribution of 7×10^{-18}. The applied frequency offsets were then modified to minimize $(f_{\text{CEO}} + \Delta f_{\text{Yb}}^*/2) - r(f_{\text{CEO}} + \Delta f_{\text{Sr}}^*/2)$, reducing this uncertainty to 3×10^{-19} for measurements from June onwards. The average uncertainty due to RF instability is 4.4×10^{-18} over all evaluated measurements, for a total fractional uncertainty of 5.4×10^{-18} resulting from the laser-to-laser link.

Gravitational frequency shift

Both clocks share the same construction and are installed on the same optical table. The stated gravitational shift correction of $-0.3(2)\times10^{-18}$ accounts for a transport distance that is 2−4 mm less for Yb than for Sr, with a positioning uncertainty of 1 mm for each clock.

Reproducibility of ratio measurements

The scatter of the individual ratio measurements does not allow us to exclude the presence of additional uncertainties. A possible cause for such an uncertainty is an excess variation in the effective lattice intensity experienced by the Yb atoms, introducing a larger light shift uncertainty than expected. This may occur partly due to a breakdown of our simplified model: We evaluate the averaged lattice light intensity for each measurement based on the observed sideband spectra (see Supplementary Fig. 1) based on a model[42] that assumes a close-to-harmonic potential, with vibrational states occupied according to a Boltzmann distribution. However, the real situation is far more complex. While the axial lattice trap depth is about 10 µK, the gravitational sag due to the lattice tilt of 15° (also see section "First-order Doppler shift") reduces the effective radial potential (supported by the beam radius of $w \approx 70$ µm) to a depth of 5 µK for ^{171}Yb atoms. The radial temperature, extracted from the model mentioned above to be 3 µK, then infers a truncated Boltzmann distribution and indicates a significant fraction of atoms sampling the anharmonic part of the radial potential. Both of these are beyond the reach of the model, and moreover, the resulting deviation may critically depend on the overlap of the independent lattice beams. For ^{87}Sr on the other hand, the atomic temperature reaches 1/10 of the lattice potential depth of ≈ 10 µK due to more effective Doppler cooling, resulting in a much more stable confinement.

If we assume that there is no additional instability, an extrapolation of the short term instability to the full measurement time yields a statistical uncertainty of 2.4×10^{-18}, for an overall ratio uncertainty of 3.6×10^{-17}.